Radial basis function collocation method solution of natural convection in porous media

Božidar Šarler and Janez Perko
Nova Gorica Polytechnic, Nova Gorica, Slovenia

Ching-Shyang Chen
University of Nevada, Las Vegas, Nevada, USA

Received November 2002
Revised January 2003

Keywords *Convection, Meshes, Polynomials, Numerical analysis*

Abstract *This paper describes the solution of a steady-state natural convection problem in porous media by the radial basis function collocation method (RBFCM). This mesh-free (polygon-free) numerical method is for a coupled set of mass, momentum, and energy equations in two dimensions structured by the Hardy's multiquadrics with different shape parameter and different order of polynomial augmentation. The solution is formulated in primitive variables and involves iterative treatment of coupled pressure, velocity, pressure correction, velocity correction, and energy equations. Numerical examples include convergence studies with different collocation point density and arrangements for a two-dimensional differentially heated rectangular cavity problem at filtration Rayleigh numbers $Ra^* = 25$, 50 and 100, and aspect ratios $A = 1/2$, 1, and 2. The solution is assessed by comparison with reference results of the fine-mesh finite volume method in terms of mid-plane velocity components, mid-plane and insulated surface temperatures, streamfunction minimum, and Nusselt number.*

1. Introduction

Understanding of transport phenomena in the porous media is of great importance in science and engineering. Ever since the original work of Darcy (1856), these phenomena have been studied both experimentally and theoretically (Sahimi, 1995). Despite the development of very sophisticated and relevant analytical techniques (Raghavan and Ozkan, 1992) a great majority of porous media models could be solved only by using discrete approximate solutions. These solutions in parallel with the development of computers nowadays allow the evaluation of physically very complex situations. However, the diversity of the involved length scales, inhomogeneities, and anisotropies, together with the justification of using different classical models (Darcy, Brinkman, Forchheimer) in a specific

A part of the present research has been supported by a NATO grant under reference PST.CLG.9977633, and bilateral Slovene-US project *Mesh-free Methods for Computational Modeling of Heat Transfer and Fluid Flow*.

International Journal of Numerical Methods for Heat & Fluid Flow
Vol. 14 No. 2, 2004
pp. 187-212

0961-5539
DOI 10.1108/09615530410513809

situation still represents a largely unresolved problem. An elaboration of the state-of-the-art in respective theoretical, experimental, and computational developments can be found in the comprehensive book of Kaviany (1995). A frequently encountered physical situation is the porous media natural convection problem, extensively treated by Nield and Bejan (1992). The problem of natural convection in the porous media was first numerically studied by Chan *et al.* (1970) by using the finite difference method (FDM). A similar study was performed approximately a decade later by Hickox and Gartling (1981) by using the finite element method (FEM). Prasad and Kulacki (1984) pioneered the use of the finite volume method (FVM) for solving this problem. Jecl *et al.* (2001) were the first to solve the problem by the boundary domain integral method (BDIM).

In recent years, a number of mesh-free methods have been developed to circumvent the problem of polygonisation encountered in the mentioned methods. In mesh-free methods, approximation is constructed entirely in terms of a set of nodes. A class of such methods is based on the collocation with radial basis functions (Golberg and Chen, 1997). These functions have been first under intensive research in multivariate data and function interpolation (Franke, 1982). Kansa (1990a, b) used them for scattered data approximation and then for the solution of the PDEs. The key point of the radial basis function collocation method or kansa method (RBFCM or KM) solution of PDEs is the approximation of the fields on the boundary and in the domain by a set of global approximation functions and subsequent representation of the partial derivatives by the partial derivatives of these global approximation functions. The discretisation is, respectively, represented only by grid-points (poles of the global approximation functions) in contrast to the FEM, FVM, BDIM methods where appropriate polygonisation needs to be generated in addition, or FDM, where points are constrained to the coordinate lines. The main advantage of using the RBFCM for solution of partial differential equations is its simplicity, applicability to different PDEs, and effectiveness in dealing with arbitrary dimension and complicated domains. The method recently started to be successfully applied in many scientific and engineering disciplines. It has been first used in heat transport context by Zerroukat *et al.* (1998) for diffusion problems and later (Zerroukat *et al.*, 2000) for advection-diffusion problems. The method has been applied to the classical De Vahl Davis natural convection problem by Šarler *et al.* (2001) and in natural convection problem with a free boundary associated with the solid-liquid phase change by Perko *et al.* (2001) by using the primitive variables. The streamfunction-vorticity formulation of the Navier-Stokes equations have been solved by RBFCM in the work of Mai-Dui and Tran-Cong (2001a).

The radial basis functions have been first put into context of porous media flow by Šarler *et al.* (2000) where the natural convection problem has been solved by the dual reciprocity boundary element method (DRBEM).

This method belongs to the semi-mesh-free methods, because the domain fields are approximated by the global interpolation with the radial basis functions and the boundary fields by the boundary elements (polygons). Present work, considered as a logical continuation of the work of Šarler *et al.* (2000), shows the possibility of solving the problem on an entirely polygon-free basis, without any boundary or domain polygonisation and subsequent cumbersome evaluation of regular, weakly-singular, strongly-singular, and hyper-singular integrals. The second principal motivation for the present research lies in the systematic assessment of the suitability of the RBFCM in recirculating flow situations. For this purpose, a comparatively simple (no convection term, no diffusion term in momentum equation) Darcy natural convection flow has been used as a starting point, which should lead to the treatment of more complicated fluid flow situations in future.

2. Governing equations

This paper deals with homogenous porous media with porosity ε and permeability $\mathscr{K}$, confined to a two-dimensional domain Ω with boundary Γ. The rigid porous matrix and the incompressible fluid with viscosity μ saturating the pores have the same constant density ϱ, effective thermal conductivity k and the specific heat at constant pressure c_{p}. The mass conservation for the defined system is

$$\nabla \cdot \mathbf{v} = 0, \tag{1}$$

where v stands for the seepage velocity. The momentum conservation is assumed to obey the Darcy law

$$0 = -\nabla P - \frac{\mu}{\mathscr{K}}\mathbf{v} + \mathbf{f}, \tag{2}$$

with P denoting pressure and f the body force. The variation of the density with temperature is included through the body force term only by using the Boussinesq approximation

$$\mathbf{f} = \varrho\mathbf{a}[1 - \beta(T - T_{\mathrm{ref}})], \tag{3}$$

where $\mathbf{a}$ stands for the acceleration vector, β for the volumetric thermal expansion coefficient, T for temperature and T_{ref} for the reference temperature. The energy conservation equation is

$$\varrho c_{\mathrm{p}} \nabla \cdot (\mathbf{v}T) = k\nabla^2 T. \tag{4}$$

The solution of the equations (1) and (2) is constructed by assuming impermeable velocity boundary conditions along the whole boundary Γ

$$\mathbf{v}\cdot\mathbf{n}_\Gamma = 0; \quad \mathbf{p}\in\Gamma, \tag{5}$$

where $\mathbf{n}_\Gamma$ stands for the normal on the boundary Γ, and $\mathbf{p}$ for the position vector. The solution of equation (4) is constructed by assuming the division of the boundary Γ into not necessarily connected parts Γ^{D} and Γ^{N} with the Dirichlet and Neumann thermal boundary conditions, respectively,

$$T = T_\Gamma; \quad \mathbf{p}\in\Gamma^{\mathrm{D}}, \quad -k\,\frac{\partial T}{\partial n_\Gamma} = F_\Gamma; \quad \mathbf{p}\in\Gamma^{\mathrm{N}}, \tag{6}$$

where T_Γ and F_Γ represent known functions. The solution of the posed natural convection problem represents the pressure, velocity, and temperature distribution over the domain Ω and the boundary Γ.

3. Solution procedure

The construction of the solution is represented in three steps. The first step involves the global approximation of the involved fields by the radial basis functions. The second step involves the set-up of collocation equations for the pressure, velocity, pressure correction, velocity correction, and temperature field, as well as the basic elements of the iterative procedure. The third step focuses on the numerical implementation issues.

3.1 Global approximation

The involved pressure, velocity, and temperatures fields are all calculated in the same grid-points $\mathbf{p}_m;\ m = 1,2,\ldots,M;\ M = M_\Gamma + M_\Omega$. The first M_Γ grid-points are distributed on the boundary and the last M_Ω in the domain. This paper is limited to the two-dimensional Cartesian system, e.g.

$$\mathbf{p} = p_\xi \mathbf{i}_\xi; \quad \xi = x,y, \tag{7}$$

where $p_\xi;\ \xi = x,y$ denote the Cartesian coordinates (base vectors $\mathbf{i}_\xi;\ \xi = x,y$) of point $\mathbf{p}$. The unknown fields are approximated by N global approximation functions $\psi_n(\mathbf{p})$ and their coefficients ς

$$\mathscr{F}(\mathbf{p}) \approx \psi_n(\mathbf{p})\varsigma_n^{\mathscr{F}}; \quad n = 1,2,\ldots,N. \tag{8}$$

The Einstein's summation convention is used in this text, i.e. any index which is repeated twice in a product is summed up. An underlined index is not summed up. Indices i, l, m, n, and ξ are introduced. They run as $i,m,l = 1,2,\ldots,M,\ n = 1,2,\ldots,N,\ \xi = x,y$ if not stated otherwise. The scalar function $\mathscr{F}$ stands for pressure, velocity component or temperature.

The approximation coefficients $\varsigma_n^{\mathscr{F}}$ can be calculated from collocation equations in points $\mathbf{p}_m$

$$\mathscr{F}(\mathbf{p}_m) \equiv \mathscr{F}_m = \psi_n(\mathbf{p}_m)\varsigma_n^{\mathscr{F}} \equiv \psi_{mn}\varsigma_n^{\mathscr{F}}. \tag{9}$$

Since the number of functions N might be chosen greater than the number of collocation points M, the following augmentation equations are needed in order to determine all the coefficients $\varsigma_n^{\mathscr{F}}$

$$\psi_n(\mathbf{p}_m)\varsigma_m^{\mathscr{F}} = 0. \tag{10}$$

Equations (9) and (10) can be written in a compact form

$$\tilde{\mathscr{F}}_i = \Psi_{in}^{\mathscr{F}}\varsigma_n^{\mathscr{F}}, \tag{11}$$

where $\tilde{\mathscr{F}}_i = \mathscr{F}_i;\ \ i = 1, 2, \ldots, M$ and $\tilde{\mathscr{F}}_i = 0;\ \ i = M+1, M+2, \ldots, N$. Coefficients ς_n follow by inverting system (11)

$$\varsigma_n^{\mathscr{F}} = \Psi_{ni}^{-1}\tilde{\mathscr{F}}_i = \Psi_{nm}^{-1}\mathscr{F}_m, \tag{12}$$

and the interpolation (8) reads

$$\mathscr{F}(\mathbf{p}) \approx \psi_n(\mathbf{p})\Psi_{nm}^{-1}\mathscr{F}_m. \tag{13}$$

The first and the second partial derivatives of the function $\mathscr{F}$ over coordinate p_ξ can be approximated as

$$\frac{\partial}{\partial p_\xi}\mathscr{F}(\mathbf{p}) \approx \frac{\partial}{\partial p_\xi}\psi_n(\mathbf{p})\Psi_{nm}^{-1}\mathscr{F}_m, \tag{14}$$

$$\frac{\partial^2}{\partial p_\xi^2}\mathscr{F}(\mathbf{p}) \approx \frac{\partial^2}{\partial p_\xi^2}\psi_n(\mathbf{p})\Psi_{nm}^{-1}\mathscr{F}_m. \tag{15}$$

3.2 Augmented radial basis functions

Two-dimensional Hardy's multiquadrics ($\lambda = 1/2$) are used in the present study

$$\psi_n(\mathbf{p}) = \left(r_n^2 + r_0^2\right)^\lambda; \quad n = 1, 2, \ldots, M, \tag{16}$$

with

$$r_n^2 = (\mathbf{p} - \mathbf{p}_{\underline{n}})\cdot(\mathbf{p} - \mathbf{p}_{\underline{n}}). \tag{17}$$

r_0 stands for the scaling parameter. The following functions are added in the first-order polynomial augmentation

$$\psi_{M+1}(\mathbf{p}) = 1, \quad \psi_{M+2}(\mathbf{p}) = \left(p_x - p_x^0\right), \quad \psi_{M+3}(\mathbf{p}) = \left(p_y - p_y^0\right), \tag{18}$$

The following three functions are added in addition to function (18) in the second-order polynomial augmentation

$$\psi_{M+4}(\mathbf{p}) = \left(p_x - p_x^0\right)^2, \quad \psi_{M+5}(\mathbf{p}) = \left(p_x - p_x^0\right)\left(p_y - p_y^0\right),$$
$$\psi_{M+6}(\mathbf{p}) = \left(p_y - p_y^0\right)^2, \tag{19}$$

The following four functions are added in addition to the functions (18) and (19) in the third-order polynomial augmentation

$$\psi_{M+7}(\mathbf{p}) = \left(p_x - p_x^0\right)^3, \quad \psi_{M+8}(\mathbf{p}) = \left(p_x - p_x^0\right)^2\left(p_y - p_y^0\right),$$
$$\psi_{M+9}(\mathbf{p}) = \left(p_x - p_x^0\right)\left(p_y - p_y^0\right)^2, \quad \psi_{M+10}(\mathbf{p}) = \left(p_y - p_y^0\right)^3. \tag{20}$$

The scaling constants p_x^0 and p_y^0 are set to

$$p_x^0 = \frac{1}{2}(p_{x^+} + p_{x^-}), \quad p_y^0 = \frac{1}{2}(p_{y^+} + p_{y^-}), \tag{21}$$

where p_{x^+}, p_{y^+} represent the maximum and p_{x^-}, p_{y^-} the minimum coordinates p_x, p_y, respectively, of the domain Ω. The polynomials have been scaled to preserve the translational symmetry of the solution. Among all RBFs tested in the review paper of Franke (1982), Hardy's multiquadrics ranked the best, followed by the Duchon's thin plate splines. The latter have been used in our preliminary study (Šarler *et al.*, 2002) of RBFCM solution of natural convection in the porous media, since they do not involve a free parameter. On the other hand, the more accurate Hardy's multiquadrics, used in the present detailed study, involve a free parameter r_0 that introduces additional degree of freedom into the present discussion. The augmentation polynomials have been included to investigate their effect on the solution.

The choice of the shape parameter remains to be a hot topic in data interpolation. Franke (1982) suggested the shape parameter to be

$$r_0 = \theta \ell, \tag{22}$$

where ℓ represents the mean distance between the grid-points and $\theta = 1.25$. On the other hand, Hardy (1990) suggested the shape parameter θ to be 0.815, where ℓ stands for the average minimum distance between the grid-points. Carlson and Foley (1991) suggested that the shape parameter increases with the increasing curvature of the interpolated function. Following this idea, Kansa (1990a) used the variable shape parameter. Golberg *et al.* (1996) proposed a statistical cross-validation technique to optimise the free parameter. Mai-Dui and Tran-Cong (2001b), Power and Barraco (2002) and Wang and Lui (2002) used sensitivity studies to find out the typical shape parameter. The latter authors employed the weak form of the Kansa method (a variant of the point interpolation method) and also adjusted the exponent λ in addition to r_0.

Mai-Dui and Tran-Cong (2001b) made a remark that their cumulative experience in determining the optimum value of θ lies somewhere between 1 and 10. A sensitivity study for determining the proper value of θ as used in the present work confirms their experience.

3.3 Solution of the pressure field

The momentum equation is coupled with the energy equation through the body force. The energy equation is coupled with the momentum equation through the velocity field. Consequently, the solution inherently involves iterations. Let us assume that the pressure, velocity, and temperature fields are all known at iteration level j. The discussion of iteration cycle that follows explains how the pressure, velocity, and temperature fields are calculated at the next iteration level j+1. The solution of the momentum equation at the iteration level j+1 is obtained in the following way. The pressure poisson equation (PPE) is constructed by taking the divergence of the momentum conservation (2)

$$\nabla^2 P^{j+1} = \nabla \cdot \left(-\frac{\mu}{\mathscr{K}} \mathbf{v}^j + \mathbf{f}^j \right). \tag{23}$$

The Neumann pressure boundary conditions can be defined along the whole boundary Γ by taking the scalar product of the momentum equation with the normal on the boundary. This gives

$$\nabla P^{j+1} \cdot \mathbf{n}_\Gamma = \left(-\frac{\mu}{\mathscr{K}} \mathbf{v}^j + \mathbf{f}^j \right) \cdot \mathbf{n}_\Gamma; \quad \mathbf{p} \in \Gamma. \tag{24}$$

Since the impermeable velocity boundary conditions (5) are valid, upper equation reduces to

$$\frac{\partial P^{j+1}}{\partial n_\Gamma} = \mathbf{f}^j \cdot \mathbf{n}_\Gamma; \quad \mathbf{p} \in \Gamma. \tag{25}$$

The pressure field is solved by approximating the PPE as follows. The collocation equations in the boundary nodes are

$$\left(\frac{\partial}{\partial p_x} \psi_{\underline{i}n} n_{\Gamma x \underline{i}} + \frac{\partial}{\partial p_y} \psi_{\underline{i}n} n_{\Gamma y \underline{i}} \right) \Psi^{-1}_{nm} P^{j+1}_m = f^j_{x\underline{i}} n_{\Gamma x \underline{i}} + f^j_{y\underline{i}} n_{\Gamma y \underline{i}}; \quad i = 1, 2, \ldots, M_\Gamma. \tag{26}$$

The collocation equations in the domain nodes are

$$\begin{aligned} \left(\frac{\partial^2}{\partial p_x^2} \psi_{in} + \frac{\partial^2}{\partial p_y^2} \psi_{in} \right) \Psi^{-1}_{nm} P^{j+1}_m &= \frac{\partial}{\partial p_x} \psi_{in} \Psi^{-1}_{nm} \left(-\frac{\mu}{\mathscr{K}} v^j_{xm} + f^j_{xm} \right) \\ &+ \frac{\partial}{\partial p_y} \psi_{in} \Psi^{-1}_{nm} \left(-\frac{\mu}{\mathscr{K}} v^j_{ym} + f^j_{ym} \right); \quad i = M_\Gamma + 1, M_\Gamma + 2, \ldots, M, \end{aligned} \tag{27}$$

where the approximation of the first and the second partial derivatives follows (equations (14) and (15)). Upper system of equations (26) and (27) is singular due to the presence of the Neumann boundary conditions over the whole boundary. One of the collocation equations in the domain nodes, denoted by N_{ref}, is represented by the reference pressure collocation equation in order to avoid the singularity

$$\delta_{N_{\text{ref}}m} P_m^{j+1} = P_{\text{ref}}; \quad M_{\Gamma+1} \leq m \leq M, \tag{28}$$

where δ stands for the Kronecker symbol and P_{ref} for the reference pressure, respectively. The solution of upper, combined boundary-domain system of equations (26)-(28) gives the unknown pressure field P_m^{j+1}. The pressure gradient field can be calculated from the pressure field through

$$\frac{\partial}{\partial p_\xi} P_m^{j+1} = \frac{\partial}{\partial p_\xi} \psi_{mn} \Psi_{nl}^{-1} P_l^{j+1}. \tag{29}$$

3.4 Solution of the velocity field

After calculating the pressure gradient field the velocity field at the iteration level $j+1$ can be explicitly calculated from the momentum equation

$$\hat{v}_{\xi m}^{j+1} = \frac{\mathscr{K}}{\mu} \left(-\frac{\partial}{\partial p_\xi} P_m^{j+1} + f_{\xi m}^{j} \right). \tag{30}$$

The "hat" on the velocity denotes that the velocity field does not correspond to the mass conservation in general. The incompressibility is enforced through the pressure $\check{P}$ and velocity corrections $\check{\mathbf{v}}$ which ensure

$$\nabla \cdot \mathbf{v}^{j+1} = \nabla \cdot (\hat{\mathbf{v}}^{j+1} + \check{\mathbf{v}}^{j+1}) = 0. \tag{31}$$

Consider that the velocity correction $\check{\mathbf{v}}^{j+1}$ occurs exclusively due to action of the pressure correction $\check{P}^{j+1}$

$$c_{\text{rel}}^{P} \frac{\mu}{\mathscr{K}} \check{\mathbf{v}}^{j+1} = -\nabla \check{P}^{j+1}, \tag{32}$$

where c_{rel}^{P} represents a heuristic velocity correction – pressure correction relaxation factor. The pressure correction can thus be calculated from the velocity field $\hat{\mathbf{v}}$ through the pressure correction poisson equation (PCPE)

$$\nabla^2 \check{P}^{j+1} = c_{\text{rel}}^{P} \frac{\mu}{\mathscr{K}} \nabla \cdot \hat{\mathbf{v}}^{j+1}, \tag{33}$$

deduced from equations (31) and (32). Since no correction is needed in the direction normal to the boundary, the following pressure correction boundary conditions are valid

$$\frac{\partial}{\partial n_\Gamma}\check{P}^{j+1} = 0. \tag{34}$$

The pressure correction field is solved by approximating the PCPE as follows. The collocation equations in the boundary nodes are

$$\left(\frac{\partial}{\partial p_x}\psi_{\underline{i}n}n_{\Gamma x\underline{i}} + \frac{\partial}{\partial p_y}\psi_{\underline{i}n}n_{\Gamma y\underline{i}}\right)\Psi^{-1}_{nm}\check{P}^{j+1}_m = 0; \quad i = 1, 2, \ldots, M_\Gamma. \tag{35}$$

The collocation equations in the domain nodes are

$$\left(\frac{\partial^2}{\partial p_x^2}\psi_{in} + \frac{\partial^2}{\partial p_y^2}\psi_{in}\right)\Psi^{-1}_{nm}\check{P}^{j+1}_m = c^P_{\text{rel}}\frac{\mu}{\mathscr{K}}\left(\frac{\partial}{\partial p_x}\psi_{in}\Psi^{-1}_{nm}\hat{v}^{j+1}_{xm} + \frac{\partial}{\partial p_y}\psi_{in}\Psi^{-1}_{nm}\hat{v}^{j+1}_{ym}\right);$$

$$i = M_\Gamma + 1, M_\Gamma + 2, \ldots, M, \tag{36}$$

where the equations (14) and (15) have been used for the approximation of the first and the second partial derivatives. Upper system of equations is singular due to the same reasons as system (26) and (27). In order to avoid the singularity, the pressure correction field is set to the reference pressure in the node N_{ref}

$$\delta_{N_{\text{ref}}m}\check{P}^{j+1}_m = P_{\text{ref}}; \quad M_\Gamma + 1 \le m \le M, \tag{37}$$

with P_{ref} standing for the reference pressure. The solution of upper, combined boundary-domain collocation system of equations (35)-(37) gives the unknown pressure correction field $\check{P}^{j+1}_m$. The pressure correction gradient field can be calculated from the pressure correction field through

$$\frac{\partial}{\partial p_\xi}\check{P}^{j+1}_m = \frac{\partial}{\partial p_\xi}\psi_{mn}\Psi^{-1}_{nl}\check{P}^{j+1}_l. \tag{38}$$

The velocity field is updated towards the incompressibility through the pressure gradient corrections

$$v^{j+1}_{\xi m} = \check{v}^{j+1}_m - \frac{\mathscr{K}}{\mu}\frac{\partial}{\partial n_\Gamma}\check{P}^{j+1}_m. \tag{39}$$

3.5 Solution of the temperature field

The iteration cycle is completed by calculating the temperature field at iteration level $j+1$ (and after that also $\mathbf{f}^{j+1}$). The energy collocation equation in the boundary nodes is

$$\left[\chi^{\mathscr{D}}_{\underline{i}}\psi_{\underline{i}n}\Psi^{-1}_{nm}+\chi^{\mathscr{N}}_{\underline{i}}\left(n_{\Gamma x\underline{i}}\frac{\partial}{\partial p_x}\psi_{\underline{i}n}\Psi^{-1}_{nm}+n_{\Gamma y\underline{i}}\frac{\partial}{\partial p_y}\psi_{\underline{i}n}\Psi^{-1}_{nm}\right)\right]T^{j+1}_m = \chi^{\mathscr{D}}_{\underline{i}}T_{\Gamma\underline{i}}+\chi^{\mathscr{N}}_{\underline{i}}F_{\Gamma\underline{i}},\quad i=1,2,\ldots,M_\Gamma, \tag{40}$$

where the boundary conditions indicator has been introduced

$$\chi^{\mathscr{D}}(\mathbf{p})=\begin{cases}1 & \mathbf{p}\in\Gamma^{\mathscr{D}}\\ 0 & \mathbf{p}\notin\Gamma^{\mathscr{D}}\end{cases},\quad \chi^{\mathscr{N}}(\mathbf{p})=\begin{cases}1 & \mathbf{p}\in\Gamma^{\mathscr{N}}\\ 0 & \mathbf{p}\notin\Gamma^{\mathscr{N}}\end{cases} \tag{41}$$

The energy collocation equation in the domain nodes is

$$\varrho c_p\nabla\cdot\left(\psi_{in}\Psi^{-1}_{nm}v^{j+1}_{\underline{m}}T^{j+1}_m\right)=k\nabla^2\psi_{in}\Psi^{-1}_{nm}T^{j+1}_m;\quad i=M_\Gamma+1,M_\Gamma+2,\ldots,M, \tag{42}$$

or explicitly

$$\left[\varrho c_{\mathrm{p}}\left(\frac{\partial}{\partial p_x}\psi_{in}\Psi^{-1}_{nm}v^{j+1}_{x\underline{m}}+\frac{\partial}{\partial p_y}\psi_{in}\Psi^{-1}_{nm}v^{j+1}_{y\underline{m}}\right)-k\left(\frac{\partial^2}{\partial p_x^2}\psi_{in}+\frac{\partial^2}{\partial p_y^2}\psi_{in}\right)\Psi^{-1}_{nm}\right]T^{j+1}_m=0. \tag{43}$$

Equations (40) and (43) may be used to solve simultaneously the unknown temperature distribution T^{j+1}_m. However, this would not permit the solution of the systems of equations to be calculated through the LU decomposition only once, since the system matrix changes due to variable velocity field. Respectively, equation (43) is numerically implemented in the following form

$$k\left(\frac{\partial^2}{\partial p_x^2}\psi_{in}+\frac{\partial^2}{\partial p_y^2}\psi_{in}\right)\Psi^{-1}_{nm}T^{j+1}_m=\varrho c_p\left(\frac{\partial}{\partial p_x}\psi_{in}\Psi^{-1}_{nm}v^{j+1}_{x\underline{m}}+\frac{\partial}{\partial p_y}\psi_{in}\Psi^{-1}_{nm}v^{j+1}_{y\underline{m}}\right)T^{j}_m, \tag{44}$$

that preserves the system matrix through all iterations. The temperature derivatives on the boundary and in the domain can be explicitly calculated as

$$\frac{\partial T^{j+1}}{\partial p_{\xi_m}}=\frac{\partial}{\partial p_\xi}\psi_{mn}\Psi^{-1}_{nl}T^{j+1}_l. \tag{45}$$

The iteration cycle is completed with the calculation of the updated body force

$$\mathbf{f}^{j+1}_m=\varrho\mathbf{a}[1-\beta(T^{j+1}_m-T_{\mathrm{ref}})]. \tag{46}$$

The iterations are stopped when conditions

$$\left|\left|\mathbf{v}_m^{j+1}\right| - \left|\mathbf{v}_m^{j}\right|\right| < v_\varepsilon, \quad \left|\left|T_m^{j+1}\right| - \left|T_m^{j}\right|\right| < T_\varepsilon, \tag{47}$$

are satisfied in all collocation points $\mathbf{p}_m$ with v_ε and T_ε representing the velocity and temperature convergence criterions. In case iteration conditions (47) are not satisfied, a new iteration cycle starts with the relaxed values of the velocity, temperature, and body force

$$\mathbf{v}_m^{j+1} = \mathbf{v}_m^{j} + c_{\text{rel}}^{\mathbf{v}}\left(\mathbf{v}_m^{j+1} - \mathbf{v}_m^{j}\right), \tag{48}$$

$$T_m^{j+1} = T_m^{j} + c_{\text{rel}}^{T}\left(T_m^{j+1} - T_m^{j}\right), \tag{49}$$

$$\mathbf{f}_m^{j+1} = \mathbf{f}_m^{j} + c_{\text{rel}}^{f}\left(\mathbf{f}_m^{j+1} - \mathbf{f}_m^{j}\right), \tag{50}$$

with c_{rel}^{v}, c_{rel}^{T}, c_{rel}^{f} representing the heuristic relaxation factors for velocity, temperature, and body force, respectively.

3.6 Numerical implementation and computer platform

The numerical implementation is made double precision in COMPAQ VISUAL FORTRAN with IMSL library. Test cases have been run on HP-OMNIBOOK XE_3 laptop with an Intel Pentium III 850 MHz processor, 256 MB memory, and MS Windows 2000 operating system. The collocation matrix Ψ has been inverted by using the routine DLINRG. The system matrix in pressure, pressure correction, and temperature systems of equations does not change. Respectively, these three systems are first LU decomposed by the routine DLFRGT and then solved by the routine DLFSRG at each iteration. The temperature and velocity iteration tolerances are set to $T_\varepsilon = 10^{-4}$, $v_\varepsilon = 10^{-4}$. Velocity relaxation factor is set to 1, temperature relaxation factor to 10^{-1}, and body force relaxation factor to 10^{-3}. The heuristic pressure correction factor is set to 1. The related criterion (47) is evaluated in all grid-points. Case "d" from Table II requires approximately 2 h of CPU time on the defined platform.

4. Numerical examples

4.1 Differentially heated rectangular cavity – scaling

Consider a rectangular impermeable cavity $p_{x^-} \le p_x \le p_{x^+}$, $p_{y^-} \le p_y \le p_{y^+}$ with heated boundary at $p_x = p_{x^-}$ and cooled boundary at $p_x = p_{x^+}$. The boundaries at $p_y = p_{y^-}$ and $p_y = p_{y^+}$ are insulated. The heated and cooled boundaries are subject to Dirichlet boundary conditions

$$T_\Gamma(p_{x^-}, p_y) = T^+, \quad T_\Gamma(p_{x^+}, p_y) = T^-. \tag{51}$$

The Neumann boundary conditions with $F_\Gamma = 0$ apply at both insulated boundaries

$$F_\Gamma(p_x, p_{y^-}) = 0, \quad F_\Gamma(p_x, p_{y^+}) = 0. \tag{52}$$

The posed classical natural convection problem can be written in a dimensionless form by defining the dimensionless coordinates $\tilde{p}_x$ and $\tilde{p}_y$

$$\tilde{p}_\xi = \frac{p_\xi - p_\xi^0}{\Delta p_\xi}, \tag{53}$$

with $\Delta p_\xi = p_{\xi^+} - p_{\xi^-}$. Cavity height/width aspect ratio A is defined as

$$A = \frac{\Delta p_y}{\Delta p_x}. \tag{54}$$

The dimensionless velocity $\tilde{\mathbf{v}}$ is defined as

$$\tilde{\mathbf{v}} = \frac{\Delta p_y}{\alpha}\mathbf{v}, \quad \alpha = \frac{k}{\varrho c_{\mathrm{p}}}, \tag{55}$$

where α stands for thermal diffusivity. The dimensionless pressure $\tilde{P}$ is defined as

$$\tilde{P} = \frac{\mathcal{K}\Delta p_y}{\alpha\mu} P. \tag{56}$$

The filtration Rayleigh number Ra* based on cavity height is defined as

$$\mathrm{Ra}^* = \frac{\varrho \mathcal{K} a \beta \Delta p_y \Delta T}{\alpha\mu}, \tag{57}$$

with $\Delta T = T^+ - T^-$. The dimensionless temperature $\tilde{T}$ is defined as

$$\tilde{T} = \frac{T - T_{\mathrm{ref}}}{\Delta T}. \tag{58}$$

The Boussinesq reference temperature is set to $T_{\mathrm{ref}} = (T^+ - T^-)/2$. The dimensionless mass and momentum conservation equations are

$$\tilde{\nabla} \cdot \tilde{\mathbf{v}} = 0, \tag{59}$$

$$0 = -\tilde{\nabla}\tilde{P} - \tilde{\mathbf{v}} + \mathrm{Ra}^* \tilde{T}\mathbf{i}_y, \tag{60}$$

with the corresponding dimensionless boundary conditions

$$\tilde{\mathbf{v}} \cdot \mathbf{n}_\Gamma = 0. \tag{61}$$

The adjacent energy equation is

$$\tilde{\nabla}\cdot(\tilde{\mathbf{v}}\tilde{T}) = \tilde{\nabla}^2\tilde{T}, \tag{62}$$

with the corresponding dimensionless boundary conditions

$$\tilde{T}_\Gamma\left(\pm\frac{1}{2}A, \tilde{p}_y\right) = \pm\frac{1}{2}, \quad \tilde{F}_\Gamma\left(\tilde{p}_x, \pm\frac{1}{2}\right) = 0. \tag{63}$$

The posed natural convection problem is completely defined through two dimensionless parameters, the aspect ratio A, and the vertical filtration Rayleigh number, Ra*.

4.2 Reference solution

Since the analytical solution to the problem is not known, the characteristics of the developed method can be assessed only by comparing it with the solution obtained by some other numerical method. The fine-mesh FVM (Gobin and Bennacer, 1996a, b) reference solution as used earlier by Šarler *et al.* (2000), is also taken as a reference in this work. The validation of the FVM code was performed over a large range of parameters for purely thermal natural convection in fluids or in porous media. The reference simulations presented hereinafter are based on the Darcy-Brinkman version of the code using a very low Darcy number, $\mathrm{Da} = 10^{-8}$. The FVM calculations were performed on a Cray-98 vector mainframe.

4.3 Discussion of the results

The main purpose of the numerical tests presented in this paper is to investigate the convergence and robustness of the developed method. The RBFCM solution is compared with the reference values of the overall cavity Nusselt number, $\mathrm{Nu}^{\mathrm{ref}}$, and streamfunction minimum, $\psi^{\mathrm{ref}}_{\mathrm{min}}$, for the five sets of dimensionless parameters listed in Table I. Six collocation point arrangements have been introduced in this work. The coarse uniform grid "a" (10×10) is composed of $M_\Gamma = 40$ boundary collocation points and $M_\Omega = 81$ domain collocation points, i.e. $M = 121$. The medium uniform grid "b" (20×20) is characterised by $M_\Gamma = 80$, $M_\Omega = 361$, $M = 441$. The fine uniform grid "c" (30×30) is characterised by $M_\Gamma = 120$, $M_\Omega = 841$, $M = 961$. The fine non-uniform grid "d" (30×30) has the same number of boundary and domain collocation points as grid "c" except that the grid-points experience the non-uniformity (defined with grid points ${}^n p_\xi, \xi = x, y$) proposed by Sadat and Couturier (2000)

$${}^n p_\xi = p_\xi^- + \frac{1}{2}\left(p_\xi^+ - p_\xi^- + \frac{\tanh[2(p_\xi - p_\xi^-) - (p_\xi^+ - p_\xi^-)]}{\tanh(1)}\right). \tag{64}$$

The uniform grid "e" (20×40) is used for calculations of the case with $A = 1/2$, and the uniform grid "f" (40×20) for calculations of the case with $A = 2$. Grids "e" and "f" are characterised by $M_\Gamma = 120$, $M_\Omega = 741$, $M = 861$.

Table II shows the accuracy of the solution in terms of streamfunction minimum and Nusselt number at $A = 1$, Ra* = 100 as a function of the free parameter θ in Hardy's multiquadrics, no polynomial augmentation. In this paper, the parameter ℓ is the interpreted as the typical mesh distance, for example in uniform Grids "a" and "b" as $\ell = \Delta p_y/10$, and $\Delta p_y/20$ in uniform grid "c" and non-uniform grid "d" as $\ell = \Delta p_y/30$, and in cases with $A = 1/2$ and 2 as $\ell = \Delta p_y/20$ and $\Delta p_y/40$, respectively. The best streamfunction accuracy is obtained with $\theta = 3$ and the best Nusselt number accuracy with $\theta = 2.5$. Since $\theta = 2.5$ requires minimum number of iterations this value has been fixed in all calculations that follow.

Table III shows the accuracy in the same measures and at the same physical conditions as Table II at fixed θ without and with polynomial augmentation. One can observe the increase in the number of required iterations to reach the convergence in cases with polynomial augmentation. Overall, the accuracy of the results does not change much with addition of the polynomial terms. This conclusion can be perceived also from the work of Power and Barraco (2002).

A	Ra*	$\mathrm{Nu}^{\mathrm{ref}}$	$\psi'^{\mathrm{ref}}_{\mathrm{min}}$
1.0	25	+1.3682	−1.6550
0.5	50	+2.1354	−2.1481
1.0	50	+1.9794	−2.8633
2.0	50	+1.3863	−2.6393
1.0	100	+3.1018	−4.7357

Note: For different aspect ratios and filtration Rayleigh numbers obtained by mesh consisting of 40,000 finite volumes

Table I.
FVM reference solution (Gobin and Bennacer, 1996a, b)

θ	Nu	$\Delta\mathrm{Nu}$	ψ'_{min}	$\Delta\psi'_{\mathrm{min}}$	J_{max}
1.0	2.7721	−0.1063	−4.2254	−0.1063	5,125
2.0	2.9762	−0.0405	−4.2808	−0.0405	3,624
2.5	3.0262	−0.0244	−4.3332	−0.0850	3,515
3.0	3.0180	−0.0270	−4.2088	−0.0270	3,592
4.0	–	–	–	–	–

Note: In terms of the Nusselt number and streamfunction minimum at $A = 1$, Ra* = 100, grid "b" as a function of multiquadric parameter θ, no polynomial augmentation. Case with $\theta = 4.0$ is not reaching convergence. $\Delta\mathrm{Nu} = (\Delta\mathrm{Nu} - \Delta\mathrm{Nu}^{\mathrm{ref}})/\Delta\mathrm{Nu}^{\mathrm{ref}}$, $\Delta\psi'_{\mathrm{min}} = (\psi'_{\mathrm{min}} - \psi'^{\mathrm{ref}}_{\mathrm{min}})/\psi'^{\mathrm{ref}}_{\mathrm{min}}$ with $\mathrm{Nu}^{\mathrm{ref}}$ and $\psi'^{\mathrm{ref}}_{\mathrm{min}}$ listed in Table I. J_{max} represents the number of required iterations for reaching convergence. The evaluation of Nu and ψ' is given in appendices 1 and 2

Table II.
Accuracy of the RBFCM solution

The polynomial augmentation was thus omitted from all subsequent calculations.

The RBFCM solution is compared with the reference solution by using the defined six grid-point arrangements.

By comparing the streamfunction and Nusselt number results in Table IV with $A = 1$ and grids "a", "b", and "c", one can observe the convergence of the results with finer grid. The non-uniform grid "d" gives better accuracy as uniform grid "c" due to redistribution of the collocation points in regions with higher field gradients, however it requires slightly more iterations to reach the convergence. The accuracy deteriorates with the higher filtration Rayleigh number which is expected due to higher gradients of the thermal and velocity fields. The number of required iterations for achieving convergence increases with the increasing A and increasing Ra* and shows almost no sensitivity to uniform grid refinement.

Figure 1 shows the flow and temperature fields. The coarse grid "a" solution shows the same principal qualitative features as the finer grids. Note the

Augmentation	Nu	ΔNu	$\psi'_{\min}$	$\Delta\psi'_{\min}$	$J_{\max}$
None	3.0262	−0.0244	−4.3332	−0.0850	3,515
First-order	3.1437	−0.0135	−4.4974	−0.0503	4,179
Second-order	3.1731	−0.0230	−4.5609	−0.0369	3,640
Third-order	3.0231	−0.0254	−4.7175	−0.0038	3,973

Note: In terms of the Nusselt number and streamfunction minimum at $A = 1$, Ra* = 100, grid "b" as a function of the order of polynomial augmentation Multiquadric parameter $\theta = 2.5$

Table III. Accuracy of the RBFCM solution

Grid type	A	Nu	ΔNu	Ra*	$\psi'_{\min}$	$\Delta\psi'_{\min}$	$J_{\max}$
a	1.0	25	1.3668	−0.0010	−1.6059	−0.0296	2,156
b	1.0	25	1.3686	+0.0003	−1.6293	−0.0155	1,958
c	1.0	25	1.3692	+0.0007	−1.6367	−0.0111	1,885
a	1.0	50	1.9344	−0.0227	−2.6871	−0.0616	2,953
b	1.0	50	1.9909	+0.0058	−2.7542	−0.0381	2,761
c	1.0	50	1.9877	+0.0042	−2.7805	−0.0289	2,699
a	1.0	100	2.6993	−0.1298	−4.1261	−0.1287	3,603
b	1.0	100	3.0262	−0.0244	−4.3332	−0.0850	3,515
c	1.0	100	3.1133	+0.0037	−4.4507	−0.0602	3,579
d	1.0	100	3.1031	+0.0004	−4.6201	−0.0244	3,832
e	0.5	50	2.1322	−0.0015	−2.1248	−0.0108	2,233
f	2.0	50	1.3840	−0.0017	−2.5999	−0.0149	2,845

Note: In terms of the Nusselt number and streamfunction minimum for different aspect ratios and filtration Rayleigh numbers as a function of collocation grid. Multiquadric parameter $\theta = 2.5$, no polynomial augmentation

Table IV. Accuracy of the RBFCM solution

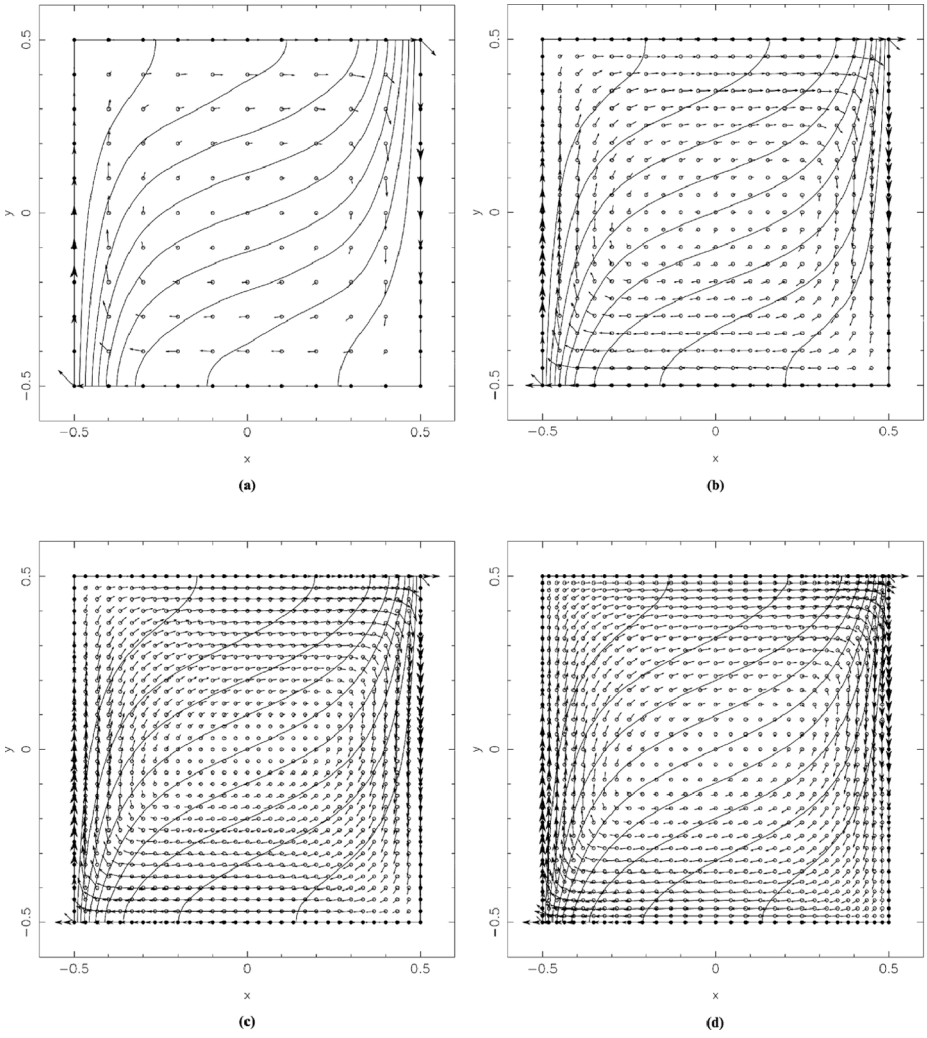

Figure 1.
Isotherms and velocity vectors for $A = 1$, $\mathrm{Ra}^{*} = 100$. The boundary grid-points are represented by • and the domain grid-points by ○. Isotherms are equidistantly spaced. From the top to the bottom: solutions with grids "a", "b", "c", and "d". Multiquadric parameter $\theta = 2.5$, no polynomial augmentation

reduction of the flow error in north-east and south-west corners as a function of grid refinement and redistribution.

Figure 2 shows the streamfunction for aspect ratios $A = 1/2$ and 2. One observes the improvement of the accuracy of the dimensionless $\tilde{v}_x$ component of the flow field in Figure 3 and dimensionless $\tilde{v}_y$ component of the flow field in Figure 4 as a function of the grid refinement. Particularly intensive is the reduction of errors in the boundary region due to grid redistribution (compare results obtained with Grids "c" and "d").

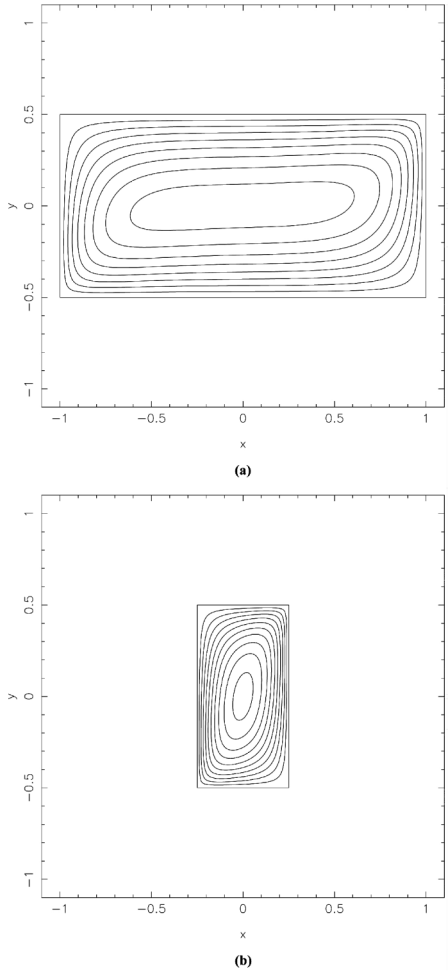

Figure 2.
Streamlines for $Ra^{*}=50$ with equidistant 0.25 step. Top $A = 1/2$, grid "e". Bottom: $A = 2$, grid "f". Multiquadric parameter $\theta = 2.5$, no polynomial augmentation

The insulated surface temperature shows large sensitivity to grid refinement and the mid-plane temperature appears to be less sensitive to the same grid refinement as shown in Figure 5.

The hot side Nusselt number shows convergence with the finer grids; however, the almost perfect match with the FVM results is obtained only with the non-uniform grid "d" (Figure 6).

5. Conclusions

This paper describes the initial attempts at solving the problem of Darcy natural convection in porous media by the RBFCM. Results are obtained for the rectangular cavities with aspect ratio 0.5, 1, and 2, and filtration Rayleigh numbers 25, 50, and 100. The method is structured on Hardy's multiquadric

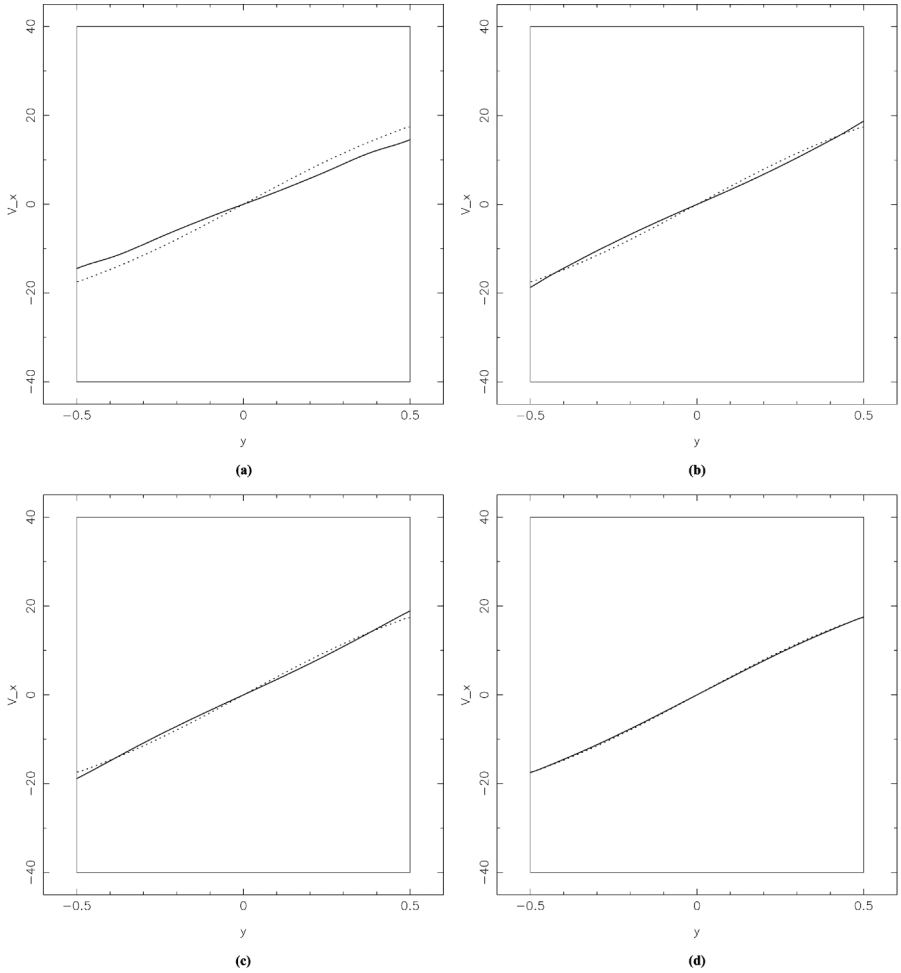

Figure 3.
Dimensionless horizontal velocity $\tilde{v}_x$ at $\tilde{p}_x = 0$ as a function of dimensionless cavity height $\tilde{p}_y$ for $A = 1$, Ra* $= 100$. Dots represent the reference fine-mesh FVM solution. From the top to the bottom: solutions with grids "a", "b", "c", and "d". Multiquadric parameter $\theta = 2.5$, no polynomial augmentation

radial basis functions. The free parameter was found to give best results at 2.5 times the typical mesh distance. Polynomial augmentation is tested in addition. The results do not differ much from the non-augmented case. The solution is shown for uniform and non-uniform grids. The calculation of streamfunction and Nusselt number from the global approximation representation of the fields leads to closed form expressions as indicated in the appendices. It has been found that the physics of the problem is qualitatively properly described even with very coarse collocation grids which quantitatively do not differ substantially from the fine-mesh FVM values. The main advantage of the method truly represents the polygon-free discretisation, simple numerical implementation, which is very similar in 2D and 3D problems, and no

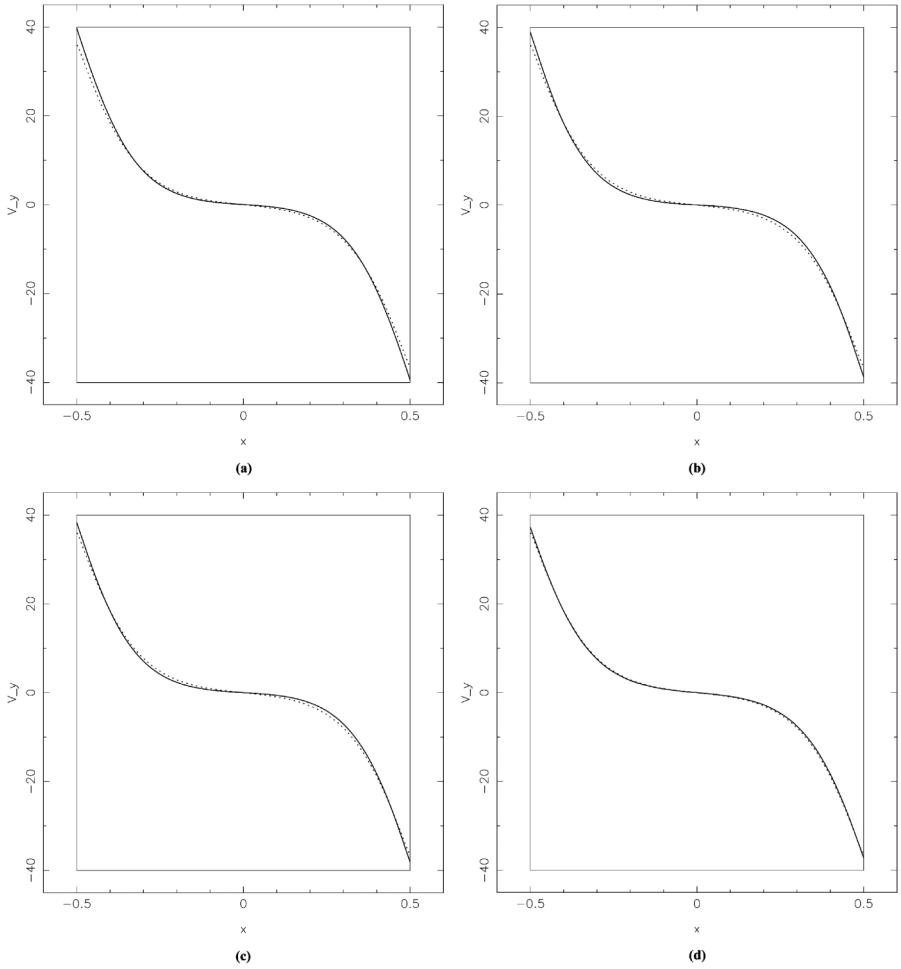

Figure 4.
Dimensionless vertical velocity $\tilde{v}_y$ at $\tilde{p}_x = 0$ as a function of dimensionless cavity width $\tilde{p}_x$ for $A = 1$, Ra* = 100. Dots represent the reference fine-mesh FVM solution. From the top to the bottom: solutions with grids "a", "b", "c", and "d". Multiquadric parameter $\theta = 2.5$, no polynomial augmentation

numerical integration involved. The method is potentially competitive because of the obvious man-power reduction in grid generation.

The formulation shown can be upgraded by the collocation that gives symmetric matrices, as recently shown by Power and Barraco (2002). Their approach is much more difficult to numerically implement, however it might have advantages in convection dominated problems. Zhang *et al.* (2000) identified the problem of poor accuracy of the derivatives at the boundary nodes in RBFCM. They introduced a Hermite type collocation method where both the PDE and boundary conditions are imposed on the boundary grid-points for improved performance. Their proposal has been further generalised by Chen and Tanaka (2000, 2002) to cope with the Dirichlet and Neumann boundary conditions as well as include the symmetric collocation.

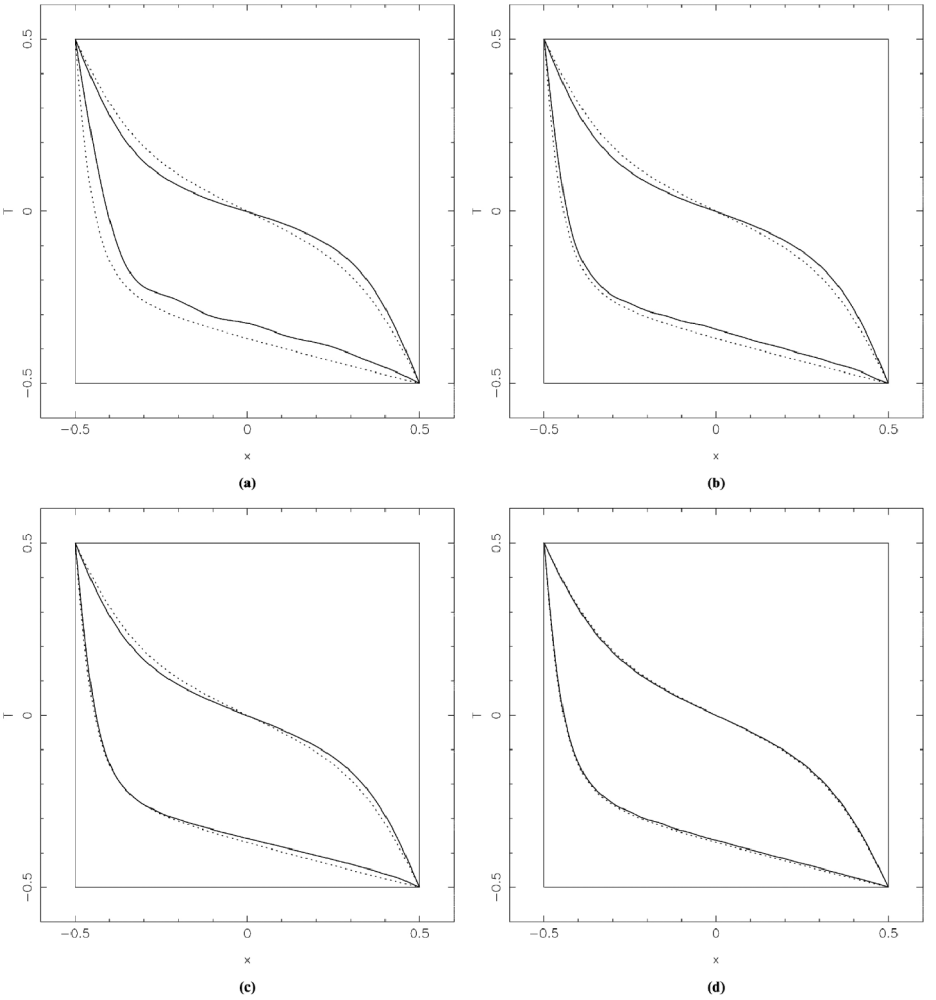

Figure 5.
Dimensionless temperature $\tilde{T}$ at $p_x = p_{x\_}$ and $\tilde{p}_x = 0$ as a function of cavity width for $A = 1$, Ra* $= 100$. Dots represent the reference fine-mesh FVM solution. From the top to the bottom: solutions with grids "a", "b", "c", and "d". Multiquadric parameter $\theta = 2.5$, no polynomial augmentation

The method of fundamental solutions with RBFs-based DRM (Li *et al.*, 2002) might replace the present Kansa solution of the involved Poisson equations. This method eliminates the second-order partial derivatives, improves accuracy, and relaxes the smoothness requirements of the RBFs used at the expense of the problems associated with positioning of the poles of the fundamental solution.

The main disadvantage of the present method represents the full involved systems of algebraic equations that are difficult and expensive to solve for large problems. This issue might be in the future mitigated by the use of the compactly supported radial basis functions, multilevel radial basis functions, iterative solvers, adaptive grid or domain decomposition. The use of compactly

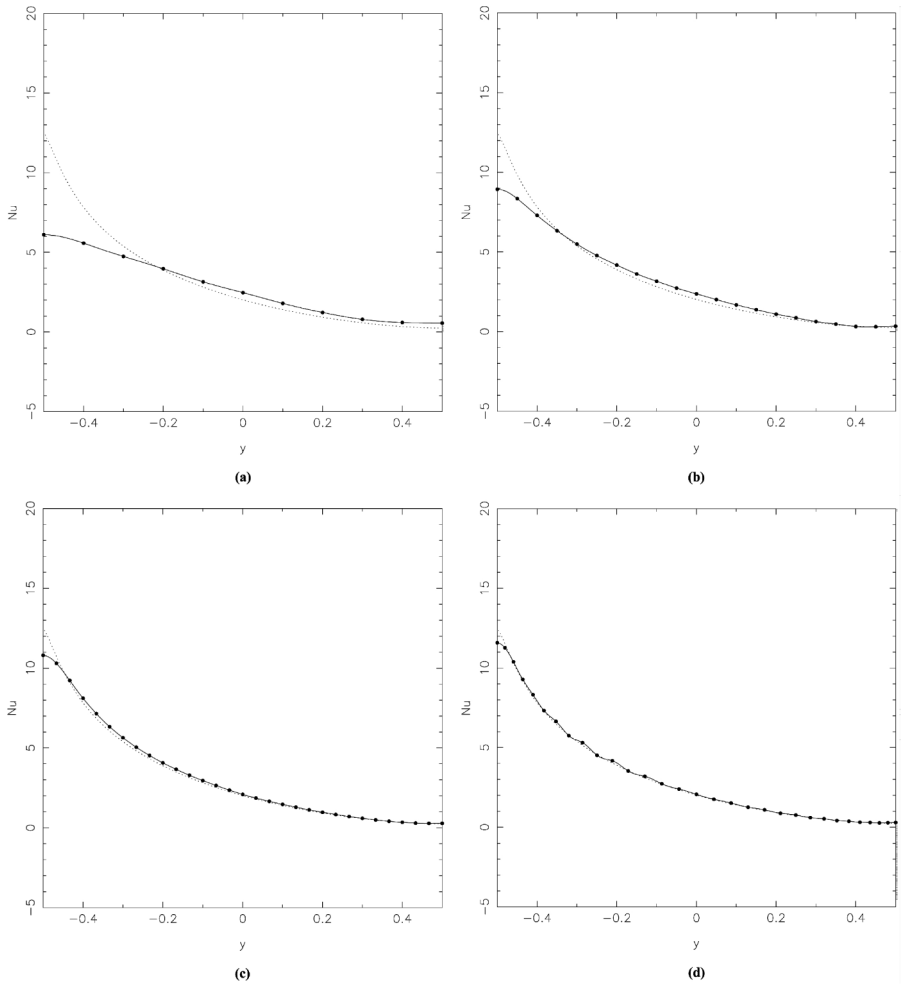

Figure 6.
Nusselt number as a function of cavity height for $A = 1$, Ra* $= 100$. Dots represent the reference fine-mesh FVM solution. Solid circles represent the calculated local Nusselt number in boundary grid-points, and the solid line denotes the calculated Nu(p_y) from the global interpolation representation of the heat flux. From the top to the bottom: solutions with grids "a", "b", "c", and "d". Multiquadric parameter $\theta = 2.5$, no polynomial augmentation

supported radial basis functions has been first proposed by Chen *et al.* (1999). The resulting matrix becomes sparse and suitable fast solvers can be employed. The multilevel radial basis functions have been introduced by Fasshauer (1999) as a mesh-free alternative to multigrid methods. The iterative solvers in connection with the RBFs have been tested by Bulgakov *et al.* (1998). The domain decomposition has been presented by Mai-Dui and Tran-Cong (2002). All mentioned approaches are possibly applicable also in the tackled porous media flow conditions.

It would be too ambitious to claim that the represented method could be extended to a wide variety of porous media situations in engineering practice at this point. Additional research is definitely required for this purpose. The listed

developments can be used as a basis to upgrade the present plain formulation of the Kansa method.

References

Bulgakov, V., Šarler, B. and Kuhn, G. (1998), "Iterative solution of systems of equations in the dual reciprocity boundary element method for diffusion equation", *International Journal of Numerical Methods in Engineering*, Vol. 43, pp. 713-32.

Carlson, R.E. and Foley, T.A. (1991), "The parameter R^2 in multiquadrics interpolation", *Computers & Mathematics with Applications*, Vol. 21, pp. 29-42.

Chan, B.K.C., Ivey, C.M. and Barry, J.M. (1970), "Natural convection in enclosed porous media with rectangular boundaries", *Wärme und Stoffübertragung*, Vol. 7, pp. 22-30.

Chen, W. and Tanaka, M. (2000), "New insights into boundary-only and domain-type RBF methods", *Journal of Nonlinear Science and Numerical Simulation*, Vol. 1, pp. 145-51.

Chen, W. and Tanaka, M. (2002), "A meshless, exponential convergence, intergation-free, and boundary-only RBF technique", *Computers & Mathematics with Application*, Vol. 43, pp. 379-91.

Chen, C.S., Brebbia, C.A. and Power, H. (1999), "Dual reciprocity method using compactly supported radial basis functions", *Communications in Numerical Methods in Engineering*, Vol. 15, pp. 137-50.

Darcy, H. *Les Fontaines Publique de la Ville de Dijon*, Victor Delmont, Paris, France.

Fasshauer, G.E. (1999), "Solving differential equations with radial basis functions: multilevel methods and smoothing", *Advances in Computational Mathematics*, Vol. 11, pp. 139-59.

Franke, J. (1982), "Scattered data interpolation: tests of some methods", *Mathematics of Computation*, Vol. 48, pp. 181-200.

Gobin, D. and Bennacer, R. (1996a), "Cooperating thermosolutal convection in enclosures, 1. Scale analysis and mass transfer", *International Journal of Heat and Mass Transfer*, Vol. 39, pp. 2671-81.

Gobin, D. and Bennacer, R. (1996b), "Cooperating thermosolutal convection in enclosures, 2. Heat transfer and flow structure", *International Journal of Heat and Mass Transfer*, Vol. 39, pp. 2683-97.

Golberg, M.A. and Chen, C.S. (1997), *Discrete Projection Methods for Integral Equations*, CMP, Southampton, UK.

Golberg, M.A., Chen, C.S. and Karur, S.R. (1996), "Improved multiquadric approximation for partial differential equations", *Engineering Analysis with Boundary Elements*, Vol. 18, pp. 9-17.

Hardy, R.L. (1990), "Theory and applications of the multiquadrics-biharmonic method (20 years of discovery 1968-1988)", *Computers & Mathematics with Applications*, Vol. 19, pp. 163-208.

Hickox, G.E. and Gartling, D.K. (1981), "A numerical study of natural convection in a horizontal porous layer subjected to an end-to-end temperature difference", *Journal of Heat Transfer*, Vol. 103, pp. 797-802.

Jecl, R., Škerget, L. and Petrišin, E. (2001), "Boundary domain integral method for transport phenomena in porous media", *International Journal for Numerical Methods in Fluids*, Vol. 35, pp. 39-54.

Kansa, E.J. (1990a), "Muliquadrics – a scattered data approximation scheme with application to computational fluid dynamics – I, Surface approximations and partial derivative estimates", *Computers & Mathematics with Applications*, Vol. 19, pp. 127-45.

Kansa, E.J. (1990b), "Muliquadrics – a scattered data approximation scheme with application to computational fluid dynamics – II, Solutions to parabolic, hyperbolic and elliptic partial differential equations", *Computers & Mathematics with Applications*, Vol. 19, pp. 147-61.

Kaviany, M. (1995), *Principles of Heat Transfer in Porous Media*, Springer-Verlag, Berlin, Germany.

Li, J.C., Hon, Y.C. and Chen, C.S. (2002), "Numerical comparisons of two meshless methods using radial basis functions", *Engineering Analysis with Boundary Elements*, Vol. 26, pp. 205-25.

Mai-Dui, N. and Tran-Cong, T. (2001a), "Numerical solution of Navier-Stokes equations using multiquadric radial basis function networks", *International Journal for Numerical Methods in Fluids*, Vol. 37, pp. 65-86.

Mai-Dui, N. and Tran-Cong, T. (2001b), "Numerical solution of differential equations using multiquadric radial basis function networks", *Neural Networks*, Vol. 14, pp. 185-99.

Mai-Dui, N. and Tran-Cong, T. (2002), "Mesh-free radial basis function network methods with domain decomposition for approximation of functions and numerical solution of Poisson's equations", *Engineering Analysis with Boundary Elements*, Vol. 26, pp. 133-56.

Nield, D.A. and Bejan, A. (1992), *Convection in Porous Media*, Springer-Verlag, Berlin.

Perko, J., Chen, C.S. and Šarler, B. (2001), "A polygon-free numerical solution of steady natural convection in solid-liquid systems", in Šarler, B. and Brebbia, C.A. (Eds), *Computational Modelling of Moving and Free Boundary Problems*, Wit Press, Southampton, UK, pp. 111-22.

Power, H. and Barraco, V. (2002), "A comparison analysis between unsymmetric and symmetric radial basis function collocation methods for the numerical solution of partial differential equations", *Computers & Mathematics with Applications*, Vol. 43, pp. 551-83.

Prasad, V. and Kulacki, F.A. (1984), "Convective heat transfer in a rectangular porous cavity – effect of aspect ratio on flow structure and heat transfer", *Journal of Heat Transfer*, Vol. 106, pp. 158-65.

Raghavan, R. and Ozkan, E. (1992), *A Method for Computing Unsteady Flows in Porous Media, Pitman Research Notes in Mathematics Series*, Vol. 318, Longman Scientific & Technical, Harlow, UK.

Sadat, H. and Couturier, S. (2000), "Performance and accuracy of a meshless method for laminar natural convection", *Numerical Heat Transfer*, Vol. 37B, pp. 455-67.

Sahimi, M. (1995), *Flow and Transport in Porous Media and Fractured Rock*, VCH Verlagsgesellschaft mbH, Weinheim, Germany.

Šarler, B., Perko, J. and Chen, C.S. (2002), "Natural convection in porous media – radial basis function collocation method solution of the Darcy model", in Mang, H.A., Rammerstorfer, F.G. and Eberhardsteiner, J. (Eds), *Proceedings of the Fifth World Congress on Computational Mechanics* (WCCM V).

Šarler, B., Perko, J., Chen, C.S. and Kuhn, G. (2001), "A meshless approach to natural convection", in Atluri, S.N. (Ed.), *International Conference on Computational Engineering and Sciences – 2001, CD-rom Proceedings*, pp. 3-9.

Šarler, B., Gobin, D., Goyeau, B., Perko, J. and Power, H. (2000), "Natural convection in porous media – dual reciprocity boundary element method solution of the Darcy model", *International Journal for Numerical Methods in Fluids*, Vol. 33, pp. 279-312.

Wang, J.G. and Liu, G.R. (2002), "On the optimal shape parameters of radial basis functions used for 2-D meshless methods", *Computer Methods in Applied Mechanics and Engineering*, Vol. 191, pp. 2611-30.

Zerroukat, M., Djidjeli, K. and Charafi, A. (2000), "Explicit and implicit meshless methods for linear advection-diffusion-type partial differential equations", *International Journal for Numerical Methods in Engineering*, Vol. 48, pp. 19-35.

Zerroukat, M., Power, H. and Chen, C.S. (1998), "A numerical method for heat transfer problems using collocation and radial basis functions", *International Journal for Numerical Methods in Engineering*, Vol. 42, pp. 1263-78.

Zhang, X., Song, K.Z., Lu, M.W., *et al.* (2000), "Meshless methods based on collocation with radial basis functions", *Comput. Mech.*, Vol. 26 No. 4, pp. 333-43.

Further reading

Chen, C.S., Ganesh, M., Golberg, M.A. and Cheng, A.H.D. (2002), "Multilevel compact radial functions based computational schemes for some elliptic problems", *Computers & Mathematics with Applications*, Vol. 43, pp. 359-78.

Golberg, M.A., Chen, C.S. and Ganesh, M. (2000), "Particular solutions of 3D Helmoltz-type equations using compactly supported radial basis functions", *Engineering Analysis with Boundary Elements*, Vol. 24, pp. 539-47.

Šarler, B. (2002), "Towards a mesh-free computation of transport phenomena", *Engineering Analysis with Boundary Elements*, Vol. 26, pp. 731-8.

Appendix 1. Calculation of streamfunction

The velocity-streamfunction ψ' relationship are

$$v_x = \frac{\partial}{\partial p_y}\psi', \quad v_y = -\frac{\partial}{\partial p_x}\psi'. \tag{65}$$

The streamfunction is calculated from the velocity components as

$$\psi' = \int_{p_{y-}}^{y} v_x \, \mathrm{d}p_y, \quad \psi' = -\int_{p_{x-}}^{x} v_y \, \mathrm{d}p_x. \tag{66}$$

A variation of the velocity components over the domain Ω and boundary Γ is based on the global approximation functions

$$v_\xi \approx \psi_n \Psi_{nm}^{-1} v_{\xi m}. \tag{67}$$

The streamfunction can be calculated as

$$\psi' = \int_{p_{y-}}^{p_y} \psi_n \, \mathrm{d}p_y \Psi_{nm}^{-1} v_{xm}, \quad \psi' = -\int_{p_{x+}}^{p_x} \psi_n \, \mathrm{d}p_x \Psi_{nm}^{-1} v_{ym}. \tag{68}$$

The involved integrals are evaluated analytically

$$\int \psi_n \, \mathrm{d}p_y = \frac{1}{9}\left(-p_y\left(6p_x^2 + p_y^2\right) + 6p_x^3 \arctan\frac{p_y}{p_x} + 3p_y\left(3p_x^2 + p_y^2\right)\log\sqrt{p_x^2 + p_y^2}\right) \tag{69}$$

$$\int \psi_{N+1} \, \mathrm{d}p_y = p_y \tag{70}$$

$$\int \psi_{N+2}\,\mathrm{d}p_y = p_y\left(p_x - p_x^0\right) \tag{71}$$

$$\int \psi_{N+3}\,\mathrm{d}p_y = p_y\left(\frac{1}{2}p_y - p_y^0\right) \tag{72}$$

$$\int \psi_{N+4}\,\mathrm{d}p_y = p_y\left(p_x - p_x^0\right)^2 \tag{73}$$

$$\int \psi_{N+5}\,\mathrm{d}p_y = p_y\left(p_x - p_x^0\right)\left(\frac{1}{2}p_y - p_y^0\right) \tag{74}$$

$$\int \psi_{N+6}\,\mathrm{d}p_y = p_y\left(\frac{1}{3}p_y^2 - p_y p_y^0 + p_y^{0^2}\right) \tag{75}$$

$$\int \psi_{N+7}\,\mathrm{d}p_y = p_y\left(p_x - p_x^0\right)^3 \tag{76}$$

$$\int \psi_{N+8}\,\mathrm{d}p_y = p_y\left(p_x - p_x^0\right)^2\left(\frac{1}{2}p_y - p_y^0\right) \tag{77}$$

$$\int \psi_{N+9}\,\mathrm{d}p_y = p_y\left(p_x - p_x^0\right)\left(\frac{1}{3}p_y^2 - p_y p_y^0 + p_y^{0^2}\right) \tag{78}$$

$$\int \psi_{N+10}\,\mathrm{d}p_y = p_y\left(\frac{1}{4}p_y^3 - p_y^2 p_y^0 + \frac{3}{2}p_y p_y^{0^2} - p_y^{0^3}\right) \tag{79}$$

Appendix 2. Calculation of Nusselt number

In the present work the local Nusselt number $\mathrm{Nu}(p_y)$ is calculated as

$$\mathrm{Nu}(p_y) = \frac{\dfrac{\partial}{\partial p_x}T(p_{x_-}, p_y)}{A\Delta T} \tag{80}$$

The overall cavity Nusselt number Nu is calculated as

$$\mathrm{Nu} = \frac{\displaystyle\int_{p_{y-}}^{p_{y+}} \frac{\partial}{\partial p_x}T(p_{x_-}, p_y)\,\mathrm{d}y}{A\Delta T} \tag{81}$$

Variation of the temperature over the domain Ω and boundary Γ is based on the global approximation functions

$$\frac{\partial}{\partial p_x}T(p_x, p_y) \approx \frac{\partial}{\partial p_x}\psi_n(p_x, p_y)\Psi_{nm}^{-1}T_m \tag{82}$$

$\mathrm{Nu}(p_y)$ can be evaluated as

$$\mathrm{Nu}_{\psi}(p_y) = \frac{\dfrac{\partial}{\partial p_x}\psi_n(p_{x_-}, p_y)\,\Psi_{nm}^{-1}T_m}{A\Delta T} \tag{83}$$

and Nu can be evaluated as

$$\mathrm{Nu} = \frac{\displaystyle\int_{p_{y_-}}^{p_{y_+}} \frac{\partial}{\partial p_x}\psi_n(p_{x_-}, p_y)\mathrm{d}p_y\Psi_{nm}^{-1}T_m}{A\Delta T} \tag{84}$$

The integrals involved are evaluated analytically

$$\int \frac{\partial}{\partial p_x}\psi_n\,\mathrm{d}p_y = p_x\left(2p_x \arctan\frac{p_y}{p_x} - p_y\left(1 - 2\log\sqrt{p_x^2 + p_y^2}\right)\right) \tag{85}$$

$$\int \frac{\partial}{\partial p_x}\psi_{N+1}\,\mathrm{d}p_y = 0 \tag{86}$$

$$\int \frac{\partial}{\partial p_x}\psi_{N+2}\,\mathrm{d}p_y = p_y \tag{87}$$

$$\int \frac{\partial}{\partial p_x}\psi_{N+3}\,\mathrm{d}p_y = 0 \tag{88}$$

$$\int \frac{\partial}{\partial p_x}\psi_{N+4}\,\mathrm{d}p_y = 2p_y\left(p_x - p_x^0\right) \tag{89}$$

$$\int \frac{\partial}{\partial p_x}\psi_{N+5}\,\mathrm{d}p_y = p_y\left(\frac{1}{2}p_y - p_y^0\right) \tag{90}$$

$$\int \frac{\partial}{\partial p_x}\psi_{N+6}\,\mathrm{d}p_y = 0 \tag{91}$$

$$\int \frac{\partial}{\partial p_x}\psi_{N+7}\,\mathrm{d}p_y = 3p_y\left(p_x - p_x^0\right)^2 \tag{92}$$

$$\int \frac{\partial}{\partial p_x}\psi_{N+8}\,\mathrm{d}p_y = 2p_y\left(p_x - p_x^0\right)\left(\frac{1}{2}p_y - p_y^0\right) \tag{93}$$

$$\int \frac{\partial}{\partial p_x}\psi_{N+9}\,\mathrm{d}p_y = p_y\left(\frac{1}{3}p_y^2 - p_y p_y^0 + p_y^{0^2}\right) \tag{94}$$

$$\int \frac{\partial}{\partial p_x}\psi_{N+10}\,\mathrm{d}p_y = 0 \tag{95}$$